Laser Phys. Lett. **7**, No. 10, 726–733 (2010) / **DOI** 10.1002/lapl.201010059

Abstract: The performance of laser-diode end-pumped Yb:LuAG microchip lasers has been investigated at ambient temperature without active cooling of the gain media. Efficient laser oscillation of Yb:LuAG crystals with different thickness and output couplings was achieved at 1030 and 1047 nm with slope efficiencies of 72 and 54%, correspondingly. The thermal population distribution at the terminated laser level of Yb:LuAG crystal plays an important role in the laser performance. The effects of the thickness of Yb:LuAG crystal and the transmission of output couplers on the laser oscillating wavelength and central wavelength shift were investigated by taking account into the reabsorption loss at lasing wavelength and intracavity laser intensity.

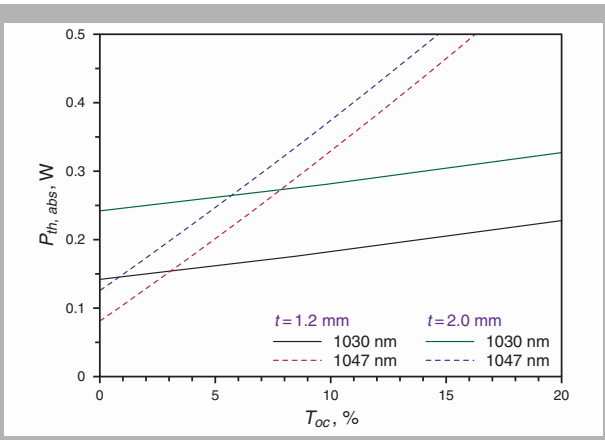

Calculated absorbed pump power thresholds of Yb:LuAG microchip lasers as a function of the transmission of the output coupler (T_{oc}) for different thickness of Yb:LuAG crystal

Laser-diode pumped efficient Yb:LuAG microchip lasers oscillating at 1030 and 1047 nm

J. Dong, [1,*] *K. Ueda,* [2] *and A.A. Kaminskii* [3]

[1] Department of Electronics Engineering, School of Information Science and Technology, Xiamen University, Xiamen 361005, China
[2] Institute for Laser Science, University of Electro-Communications, 1-5-1 Chogugaoka, Chofu, Tokyo 182-8585, Japan
[3] Institute of Crystallography, Russian Academy of Sciences, Moscow 119333, Russia

Received: 10 June 2010, Revised: 14 June 2010, Accepted: 17 June 2010
Published online: 20 July 2010

Key words: Yb:LuAG crystal; microchip laser; wavelength shift

1. Introduction

Ytterbium doped laser materials have been intensely investigated for developing high power laser-diode pump solid-state lasers, tunable lasers and femtosecond lasers around 1 μm [1–3]. Yb:YAG as crystals and polycrystalline ceramics are one of the dominant laser gain media used for solid-state lasers [4–7] owing to the excellent optical, thermal, chemical and mechanical properties [8]. Yb:YAG crystals have been used as gain medium to obtain high average output power short-pulse generation in laser-diode pumped regenerative amplifier [9]. And circular modes selection in Yb:YAG laser has been demonstrated by using intracavity lens with spherical aberration [10]. Efficient high peak power passively Q-switched Yb:YAG lasers with Cr^{4+}:YAG or semiconductor saturable absorber mirror (SESAM) as saturable absorber have been demonstrated [11–13]. Also actively Q-switched Yb:YAG lasers have been demonstrated [14].

Another interest in Yb:YAG lasers is that the frequency doubled wavelength of 515 nm matches the highest power line of Ar-ion lasers, thereby leading to the possibility of an all solid-state replacement [15]. Frequency doubling could be realized either placing appropriate nonlinear crystals inside or outside of the resonator. Intracavity frequency doubling is a well-developed way to

* Corresponding author: e-mail: jdong@xmu.edu.cn

convert fundamental wavelength of laser-diode pumped Yb:YAG lasers to green light in the continuous-wave operation with different frequency doubling nonlinear crystals [16–18]. The high peak power generation in passively Q-switched Yb:YAG lasers provide another advantage to construct simple and robust extracavity frequency doubling laser sources, and efficient 515 nm frequency doubling green light has been demonstrated in passively Q-switched Yb:YAG/Cr^{4+}:YAG microchip laser [19]. The temperature dependent and Yb doping concentration dependent optical properties and laser performance have been investigated systematically in Yb:YAG crystals and ceramics recently [20], the results show that better laser performance can be achieved with highly doped Yb:YAG ceramics other than Yb:YAG crystals. Because the thermal and optical properties of Yb:YAG crystal have been improved dramatically at low temperature [21,22], therefore laser performance of Yb:YAG materials can be improved dramatically at cryogenic temperature. Efficient laser performance of cryogenically-cooled Yb:YAG lasers has been demonstrated [23–25].

Although Yb:YAG laser materials have been widely used in solid-state lasers, the measured peak effective emission cross section for Yb:YAG is relatively modest compared to other hosts [26,27]. Therefore, investigation of other ytterbium doped laser crystals with good optical, thermal properties is still an interesting topic in the solid-state laser fields, and a similarly robust host material with more favorable emission cross section is desired for laser applications. Among more than 230 oxide and fluoride laser host-crystalline materials, the lutetium compounds (at present about 30 species) are of special interest [28]. In particular, as substitution of yttrium by lutetium ions in several structures, the lutetium compounds are preferable for trivalent lanthanide lasants (Ln^{3+}). For example, the tetragonal Ln^{3+}:$LiLuF_4$ laser crystals are congruently melted, while the isostructural Ln^{3+}:$LiYF_4$ fluorides are incongruently melted laser crystals [29, 30]. In the case of Ln^{3+}-doped laser orthorhombic $YAlO_3$ [31] and $LuAlO_3$ [32], the later is more stable during growing process due to advantages related phase diagrams. For Nd^{3+}-doped $Y_3Al_5O_{12}$ and $Lu_3Al_5O_{12}$ laser garnets, the latter offers more suitable properties for laser action due to relatively small Stark splitting of the metastable $^4F_{3/2}$ state of lasant ions [33]. In the case of Ln^{3+}-doped Y_2O_3 and Lu_2O_3 single crystals, the latter have not polymorphic transition, where the Yb^{3+}:Lu_2O_3 sesquioxide offers record broad tunable lasing spectral range for ytterbium crystals [34]. From historical point of view, the first laser lutetium crystals were $Lu_3Al_5O_{12}$, $LuAlO_3$, and $Lu_3Sc_2Al_3O_{12}$ doped with several Ln^{3+} ions (see, e.g. [35–38]). It is asserted that lutetium laser crystals are special chapter in modern material science. At now the Yb^{3+}:$Lu_3Al_5O_{12}$ (Yb:LuAG) crystal becomes one of the important laser materials for developing laser-diode (LD) pumped solid-state lasers [8,39] because it has large emission peak cross-section compared to that for Yb:YAG crystal [39]. Yb:LuAG also has comparable mechanical properties such as high thermal conductivity to that of Yb:YAG crystal [40]. The other interesting characteristics of Yb:LuAG crystal is that it has very strong absorption at 968 nm wavelength, which is higher than that at 940 nm, therefore, high quantum efficiency can be achieved by using 968-nm LD as pumping source. Optical properties of Yb:LuAG and LD pumped Yb:LuAG was reported at room temperature [39]. And thorough investigation of temperature dependent laser performance of Yb:LuAG crystal under 970 nm LD pumping was performed [41]. More recently, crystal growth, spectroscopic and laser properties of Yb:LuAG crystals doped with various Yb concentrations were investigated [40]. The results show that Yb:LuAG crystal with large emission cross section will be more suitable for ultrashort pulse generation. Efficient passively Q-switched Yb:LuAG microchip lasers with over 40% slope efficiency have been demonstrated, laser pulses with pulse width of 610 ps have been obtained [42]. Continuous-wave tunable laser operating from 1033–1079 nm and passively mode-locked laser operation with pulse width of 7.63 ps have been reported in laser-diode pump Yb:LuAG lasers [43]. However, even with optimum output coupling of 15% transmission, slope efficiency of only 42.7% was achieved with respective of the absorbed pump power for continuous-wave (CW) operation. The performance of Yb:LuAG lasers still has space to be improved. Microchip laser is one of the efficient configurations to realize efficient laser performance at ambient temperature. For certain Yb doping concentration, the thickness of Yb:LuAG crystal, the output coupling are two factors governing the laser performance. However, up to now, there is no reports about the effect of the thickness of Yb:LuAG crystal and output coupling on the Yb:LuAG microchip lasers without active cooling of the gain medium at ambient temperature.

In this paper, the efficient laser performance of Yb:LuAG microchip lasers at ambient temperature was presented. The effects of thickness of Yb:LuAG crystal and output couplings on the performance of Yb:LuAG microchip lasers were investigated and the performance of Yb:LuAG microchip laser indicated that better laser performance can be realized by choosing suitable thickness in this gain medium and output coupling transmission. We demonstrated that microchip laser can oscillate efficiently at 1030 and 1047 nm by using 5 at.% Yb:LuAG crystal. The laser properties become worse with the thickness of Yb:LuAG crystal owing to enhanced reabsorption with thickness of Yb:LuAG crystal and the strong thermal population distribution.

2. Optical properties of Yb:LuAG crystal

The Yb:LuAG crystal used in the experiments was grown by traditional Czochralski (CZ) method, with a Yb^{3+}-ion doping concentration of 5 at.%. The crystal was grown along the $\langle 111 \rangle$ axis direction. The absorption and emission spectra of Yb:LuAG crystal were measured at room

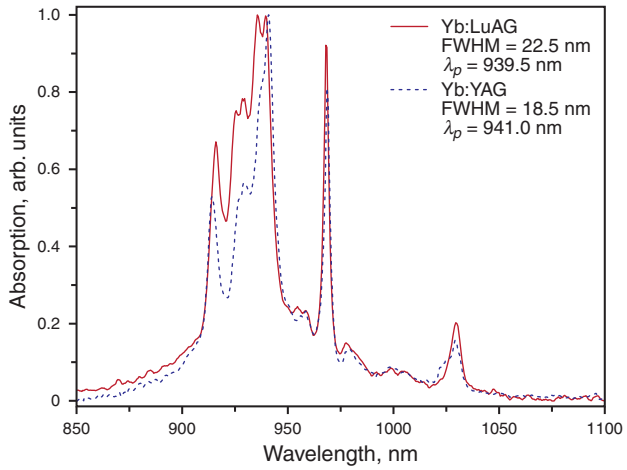

Figure 1 (online color at www.lphys.org) Absorption spectrum of Yb:LuAG crystal doped with 5 at.% Yb^{3+}-ions at room temperature, the absorption spectrum of Yb:YAG doped with 5 at.% Yb^{3+}-ions is also plotted for comparison

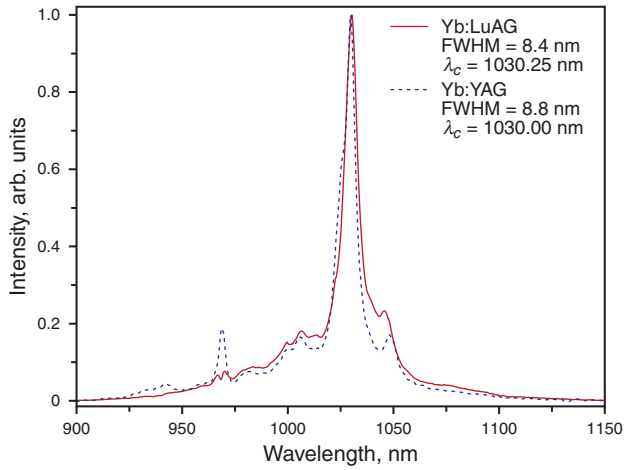

Figure 2 (online color at www.lphys.org) Emission spectrum of Yb:LuAG crystal doped with 5 at.% Yb^{3+}-ions at room temperature. The emission spectrum of Yb:YAG crystal is shown for comparison

temperature. A Yb:YAG crystal doped with 5 at.% Yb was also used to compare the optical properties with those of Yb:LuAG crystal. The absorption spectra of Yb:LuAG and Yb:YAG crystals are shown in Fig. 1. There are four absorption peaks centered at 916.0, 939.5, 968.0, and 1030.0 nm, respectively, which are similar to those of Yb:YAG crystal. 916.0, 939.5, and 968.0 nm are suitable for laser-diode pumping. However, there are some differences between Yb:LuAG and Yb:YAG crystals. There is a doublet absorption peak centered at 935.5 and 939.5 nm, respectively, and it looks like a top-flat profile with 4 nm width. The peak absorption wavelength centered at 939.5 nm is about 1.5 nm blue-shift comparing to that for Yb:YAG crystal. The absorption bandwidth (FWHM) of Yb:LuAG crystal centered at 939.5 nm was measured to be 22.5 nm, which is about 1.3 times wider than that for Yb:YAG crystals [44]. Therefore, the Yb:LuAG crystal is more suitable for 940-nm laser-diode pumping owing to the broader band absorption features. The absorption coefficient at 939.5 nm is 6 cm^{-1}. The absorption at 968 nm of Yb:LuAG crystal is higher than that of Yb:YAG crystal, which is more suitable for 968 nm laser-diode pumping. Fig. 2 shows the room temperature emission spectra of Yb:LuAG crystal containing 5 at.% of ytterbium activators. The emission spectra of Yb:LuAG crystal is similar to that of Yb:YAG single crystals. Two main emission peaks are centered at 1030.25 nm and 1046.00 nm, the effective emission intensity at 1030.25 nm is about 4.3 times of that at 1046.00 nm. The emission bandwidth centered at 1030.25 nm ($\sim$8.4 nm) is the same as that of Yb:YAG crystal. The emission shift to longer wavelength of Yb:LuAG crystal is caused by the weakening of crystal field by the substitution of the Al^{3+} ion by larger Lu^{3+} ions [45]. The fluorescence lifetime was measured to be 1.1 ms owing to the radiative trapping effect in the lifetime measurement for ytterbium doped materials, which is longer than that of Yb:YAG crystals ($\sim$0.951 ms [46]).

The absorption cross-section spectrum of Yb:LuAG crystal was calculated by using the absorption spectrum of Yb:LuAG and the concentration of Yb^{3+}-ion in the Yb:LuAG crystal. The effective emission cross-section spectrum was estimated by using the Fuchtbauer-Ladenburg (F-L) formula and measured fluorescence lifetime of the Yb:LuAG crystal. Therefore, the gain cross-section of the Yb:LuAG crystal was determined from the absorption and emission cross-section spectra of Yb:LuAG crystal under different population inversion ratio, $\beta = N_2/N_0$, N_2 is the inversion population and N_0 is the total population of Yb^{3+}-ions in Yb:LuAG crystal. The gain cross-section spectra of Yb:LuAG can be expressed as $\sigma_g(\lambda) = \beta\sigma_e(\lambda) - (1-\beta)\sigma_a(\lambda)$. $\sigma_e(\lambda)$ and $\sigma_a(\lambda)$ are the emission and absorption cross-section of the Yb:LuAG crystal, respectively. Fig. 3 shows the gain cross-section, $\sigma_g(\lambda)$, of Yb:LuAG crystal for different values of population inversion ratio, β. The absorption cross-section spectrum was obtained when β was set to 0; and the emission cross-section spectrum was obtained when β was set to 1. Absorption cross-section peaks are located near 935.5 and 939.5 nm, with a value of 0.73×10^{-20} cm^2, and emission cross-section peak is located near 1030.25 nm, with a value of $\sim 2.8\times10^{-20}$ cm^2, which is higher than that of Yb:YAG crystal (about 2.3×10^{-20} cm^2) [22]. It is worth noting that there is another absorption peak near 968 nm, which is also useful for optical pumping for realizing high quantum efficiency laser operation. We also note that the emission spectrum extends up to nearly 1150 nm, which is promising for the development of new broadly tunable

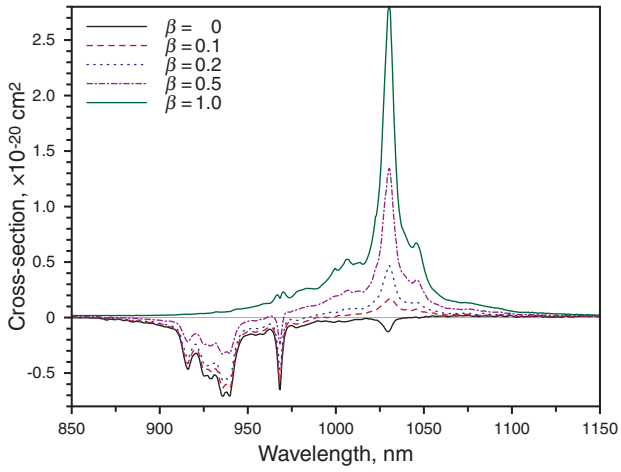

Figure 3 (online color at www.lphys.org) Gain cross-section, $\sigma_g(\lambda)$ of Yb:LuAG crystal for different values of population inversion ratio, $\beta = N_2/N_0$. $\sigma_g(\lambda) = \beta\sigma_e(\lambda) - (1-\beta)\sigma_a(\lambda)$. $\sigma_e(\lambda)$ and $\sigma_a(\lambda)$ are the emission and absorption cross-section of Yb:LuAG crystal, respectively. Absorption cross-section spectrum was obtained when β was set to 0; emission cross-section spectrum was obtained when β was set to 1

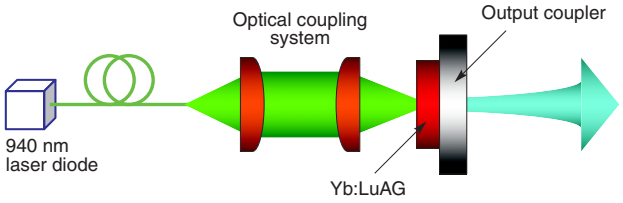

Figure 4 (online color at www.lphys.org) Schematic diagram of laser-diode pumped Yb:LuAG microchip lasers

laser sources, as well as for the design of femtosecond oscillators or amplifiers.

3. Laser experiments

The laser experiment was carried out with plane-parallel, 1.2- and 2.0-mm-thick LuAG crystal plates doped with 5 at.% Yb^{3+} ions as gain media. The cross-section of the gain medium is 6×6 mm^2. The schematic diagram of experimental setup is shown in Fig. 4. One surface of these plates is anti-reflection-coated at 940 nm and highly reflecting at 1030 nm to act as a cavity mirror of the laser. The other surface is anti-reflection-coated at lasing of 1030 nm to reduce the cavity loss. Four plane-parallel mirrors were used as output couplers with different transmissions (T_{oc}) of 5, 10, 15, and 20% at 1.03 μm. The overall cavity length was the thickness of the gain crystal. The mechanically contacted Yb:LuAG crystal and output coupler were held between two copper blocks with an aperture

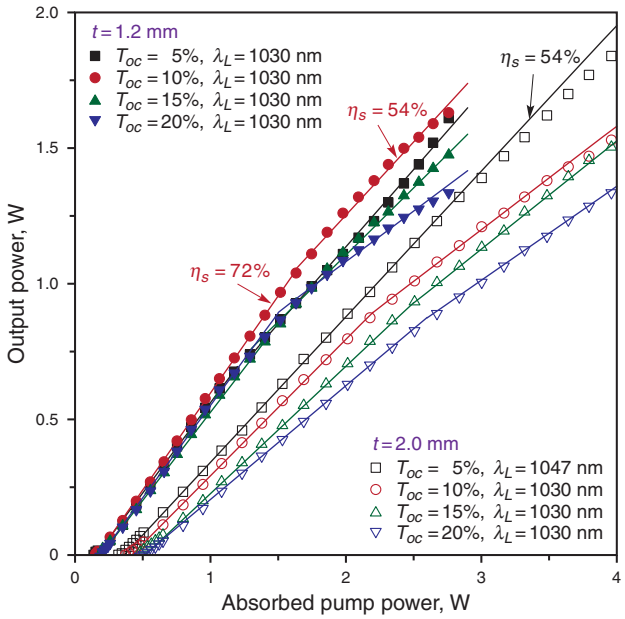

Figure 5 (online color at www.lphys.org) Output power of Yb:LuAG microchip lasers as a function of the absorbed pump power with different thickness and output couplings. The solid lines show the linear fitting of experimental data

of 3 mm in diameter. A high power fiber-coupled 940 nm LD with a core diameter of 100 μm and numerical aperture of 0.22 was used as the pump source. Two lenses with 8-mm focal length were used to focus the pump beam on the Yb:LuAG crystal rear surface and to produce a pump light footprint in the crystal of about 100 μm in diameter. About 95% of the total pumping power is incident on the Yb:LuAG crystal plate after the coupling optics. The microchip lasers operated at room temperature without active cooling of the active element. The spectral composition of these lasers was analyzed with an optical spectrum analyzer (ANDO AQ6137).

4. Results and discussion

The output power of Yb:LuAG microchip lasers as a function of the absorbed pump power for different output couplings and different thicknesses of Yb:LuAG crystals is shown in Fig. 5. The absorbed pump power thresholds of 2.0-mm-thick microchip lasers are 0.33, 0.38, 0.47, and 0.49 W for T_{oc} = 5, 10, 15, and 20%, respectively. The absorbed pump power thresholds of 1.2-mm-thick microchip lasers are 0.14, 0.15, 0.18, and 0.20 W for T_{oc} = 5, 10, 15, and 20%, respectively, which are lower than those for 2.0-mm-thick Yb:LuAG lasers. The output power increases linearly with the absorbed pump power when the pump power is well above the pump power threshold for 2.0-mm-thick Yb:LuAG plate, which is the nature of quasi-three-level operating scheme, the high efficiency can be

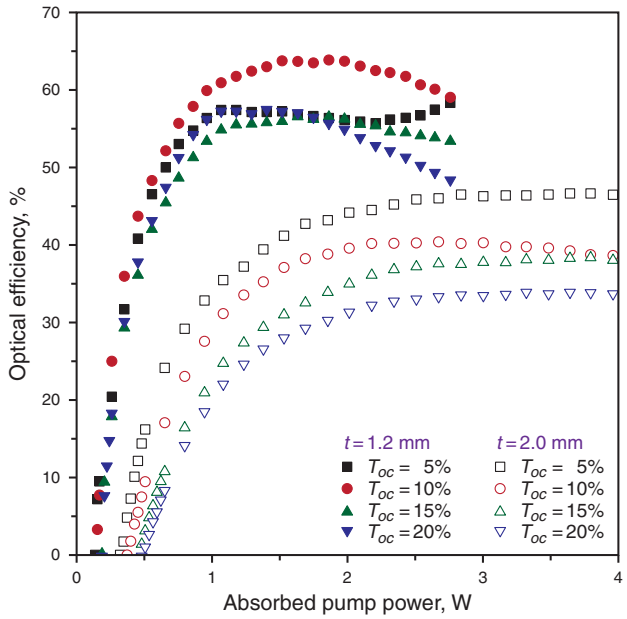

Figure 6 (online color at www.lphys.org) Optical-to-optical efficiency of Yb:LuAG crystal microchip laser as a function of absorbed pump power with different thickness of Yb:LuAG crystal and transmissions of the output coupler

achieved by using high pump power intensity. The slope efficiencies are 54, 50, 47, and 42% for $T_{oc}=5$, 10, 15 and 20%, respectively. The maximum output power of 1.84 W was measured for $T_{oc}=5\%$ when the absorbed pump power was 4.0 W, the corresponding optical-to-optical efficiency was about 46%. The output power decreases with increase of the transmission of output couplers. And there is a tendency of decreasing the slope efficiency for $T_{oc}\geq 10\%$, which is caused by the thermal effect induced by the temperature rise owing to the heat generated by the absorbed pump power at high pump power level for 1030 nm oscillations. The performance of 1.2-mm-thick microchip laser is better than that of 2.0-mm-thick Yb:LuAG plate (as shown in Fig. 5). The output power increases linearly with absorbed pump power for $T_{oc}=5$, 10, 15, and 20% although the output power increases slowly with absorbed pump power when the absorbed pump power is higher than 1.7 W. The slope efficiencies were measured to be 68, 72, 65, and 68% for $T_{oc}=5$, 10, 15, and 20%, then changed to 57, 54, 49, and 37% when the absorbed pump power is higher than 1.7 W. Maximum output power of 1.63 W was measured for $T_{oc}=10\%$ when the absorbed pump power was 2.8 W, the corresponding optical-to-optical efficiency is 58%. The performance (slope efficiency and optical-to-optical efficiency with respective to the absorbed pump power) of 5 at.% Yb:LuAG microchip lasers are better than those obtained in 10 at.% Yb:LuAG laser with optimum output coupling of 15% transmission [43].

Fig. 6 shows the optical efficiency of Yb:LuAG microchip laser as a function of the absorbed pump power for different thicknesses of Yb:LuAG crystal. The optical efficiency increases with the absorbed pump power and tends to be saturated when the absorbed pump power is higher than 2.5 W for 2.0-mm-thick Yb:LuAG microchip lasers. However, there is a maximum optical efficiency of 1.2-mm-thick Yb:LuAG lasers for all the output couplings (as shown in Fig. 6). The optical-to-optical efficiency decreases with a further increase of the pump power owing to the thermal effect in the gain medium. Maximum optical efficiency of 63.8% was achieved at the absorbed pump power of 1.5 W for 1.2-mm-thick Yb:LuAG crystal; Maximum optical efficiency of 46.6% was measured at the absorbed pump power of 3.6 W for 2.0-mm-thick Yb:LuAG crystal. The decrease of the optical efficiency with the thickness of Yb:LuAG crystal was caused by reabsorption loss with the thickness of Yb:LuAG crystal.

Measured laser emitting spectra show that Yb:LuAG microchip lasers oscillate at multilongitudinal modes. The number of the longitudinal modes increases with absorbed pump power for all the cases (different thicknesses of Yb:LuAG and different output couplings). For 1.2-mm-thick Yb:LuAG microchip lasers, the lasers oscillate around 1030 nm for different output couplings, and central emitting wavelength shifts to longer wavelength with absorbed pump power. For 2.0-mm-thick Yb:LuAG crystal, laser oscillates around 1047 nm for $T_{oc}=5\%$, the central wavelength shifts to longer wavelength with absorbed pump power. The laser oscillates at 1030 nm for $T_{oc}=10$, 15, and 20%. The oscillation wavelength difference between 1.2 and 2.0 mm thick Yb:LuAG microchip lasers for $T_{oc}=5\%$ is attributed to the different laser thresholds. The pump power threshold of quasi-three-level laser including the reabsorption loss can be expressed [6,25]

$$P_{th}=\frac{h\nu_p\pi\left(w_p^2+w_L^2\right)\left(L+T_{oc}+2\sigma f_{low}N_{tot}l\right)}{4\eta_a\tau\sigma}, \quad (1)$$

where h is the Planck constant, ν_p is the frequency of pump power, w_p and w_L are the beam waist of pump beam and laser beam, L is the intracavity loss including the diffraction loss and scattering losses, σ is the emission cross-section of gain medium at lasing wavelength, τ is the fluorescence lifetime of gain medium, l is the length of the gain medium, f_{low} is the thermal population distribution factor at terminated laser level, N_{tot} is the total population of Yb^{3+} ions in gain medium, $\eta_a=1-\exp(-\alpha l)$, is the absorption efficiency of pump power, α is the absorption coefficient of gain medium at pump wavelength.

Based on the estimated cavity loss and the threshold formula including the reabsorption loss at laser wavelength for quasi-three-level system [47,48], the absorbed pump power threshold at both laser wavelengths (1030 and 1047 nm) as a function of the transmission of the output couplers is shown in Fig. 7. The pump power threshold for both laser wavelengths increases with the transmission of the output coupler, however the pump power threshold

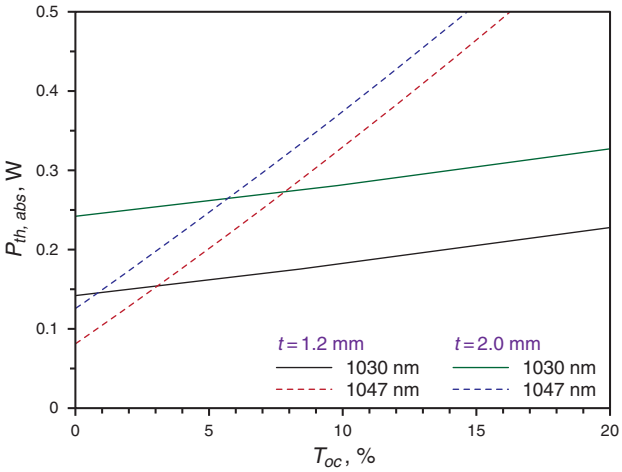

Figure 7 (online color at www.lphys.org) Calculated absorbed pump power thresholds of Yb:LuAG microchip lasers as a function of the transmission of the output coupler (T_{oc}) for different thickness of Yb:LuAG crystal

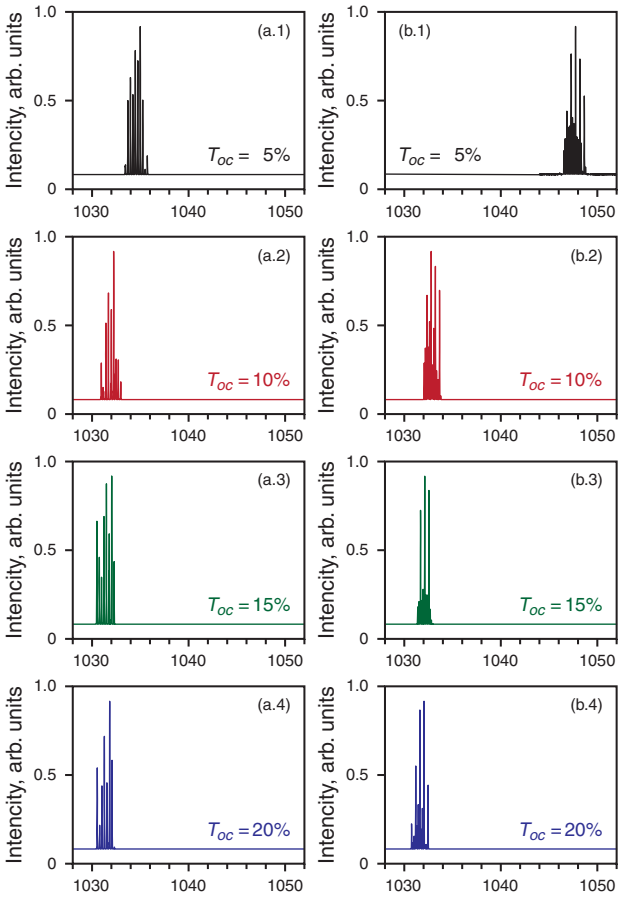

Figure 8 (online color at www.lphys.org) Laser spectra of Yb:LuAG microchip lasers with different output couplings for (a) – 1.2-mm-thick Yb:LuAG at P_{abs} = 2.8 W and (b) – 2.0-mm-thick Yb:LuAG at P_{abs} = 4.0 W

for 1047 nm increases faster than that for 1030 nm owing to the emission cross section at 1047 nm of Yb:LuAG is only a quarter of that at 1030 nm. For 1.2-mm-thick Yb:LuAG crystal, when the transmission of the output coupler is smaller than 3%, the threshold at 1047 nm is lower than that at 1030 nm because of the thermal distribution factor at 762 cm^{-1} is less than half of that at 600 cm^{-1} for Yb:LuAG crystal. Therefore, under the same laser cavity configuration, when the transmission of the output coupler is greater than 3%, Yb:LuAG laser oscillates at 1030 nm preferentially instead of 1047 nm. However, for 2.0-mm-thick Yb:LuAG crystal, the absorbed pump power threshold at 1047 nm is lower than that at 1030 nm when T_{oc} is less than 5.5%, therefore, 2.0-mm-thick Yb:LuAG microchip laser oscillated at 1047 nm preferably for $T_{oc} = 5\%$, and oscillated at 1030 nm for $T_{oc} \geq 10\%$. The laser action around 1047 nm for 2.0-mm-thick LuAG with lower transmission of output coupler ($T_{oc} = 5\%$) is attributed to the thermal population distribution in its terminated laser level, the thermal population of these levels is proportional to the thickness of Yb:LuAG. These calculations are in good agreement with the Yb:LuAG laser experimental results for different transmissions of the output couplers.

Fig. 8 shows the typical laser emitting spectra of Yb:LuAG microchip lasers for different output couplings under maximum available absorbed pump power (e.g. 2.8 W for 1.2-mm-thick Yb:LuAG plate and 4.0 W for 2.0-mm-thick Yb:LuAG plate). The separation of two close longitudinal modes was about 0.25 nm for 1.2-mm-thick Yb:LuAG lasers. The separation of two close longitudinal modes was measured to be 0.15 nm for 2.0-mm-thick Yb:LuAG microchip lasers. The different intensity of each longitudinal modes shows there is strong mode hoping and mode-competition between longitudinal modes. The linewidth at each mode was measured to be less than 5.7 GHz, i.e. the resolution limit of used instrument. The separation of the longitudinal modes in a laser cavity was given by [49] $\Delta\lambda = \lambda^2/(2L_c)$, where L_c is the optical length of the resonator. For 2.0-mm-thick planar-parallel Yb:LuAG gain medium studied here, $\Delta\lambda$ was calculated to be 0.152 and 0.153 nm with the laser wavelength of 1030 and 1047 nm, respectively, which were in good agreement with the experimental data. For 1.2-mm-thick planeparallel Yb:LuAG gain medium, $\Delta\lambda$ was calculated to be 0.26 nm with the laser wavelength of 1030 nm, which were also in good agreement with the experimental data.

The dependence of central emitting wavelength of Yb:LuAG microchip lasers on the intracavity intensity based on the measured output power was shown in Fig. 9. For 1.2-mm-thick Yb:LuAG crystal, the central wavelength shifts to longer wavelength with intracavity intensity for different output couplings. There is 4.45 nm shift from 1030.02 to 1034.47 nm for 1.2-mm-thick Yb:LuAG

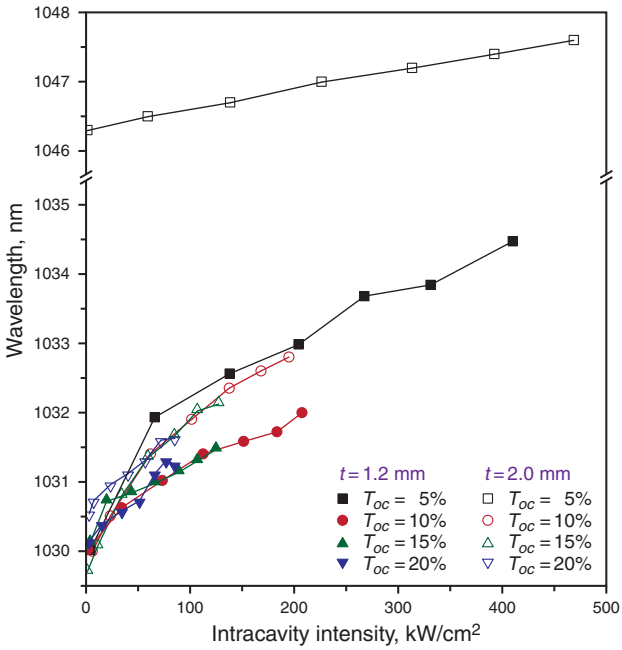

Figure 9 (online color at www.lphys.org) Central wavelength shift with intracavity intensity of microchip Yb:LuAG lasers

microchip laser with $T_{oc} = 5\%$, the wavelength shift becomes less significant for the high transmission of the output couplers (e.g. 2.00, 1.35, and 1.10 nm for $T_{oc} = 10$, 15, and 20%, respectively). For 2.0-mm-thick Yb:LuAG crystal, the central wavelength shifts from 1046.3 to 1047.6 nm for $T_{oc} = 5\%$ when the intracavity intensity of the lasers increases from the threshold values to 470 kW/cm^2. For $T_{oc} \geq 10\%$, the laser oscillates around 1030 nm, the central wavelength shifts to longer wavelength with intracavity intensity, and becomes less significant with intracavity intensity (e.g. 2.8, 2.4, and 1.1 nm for $T_{oc} = 10$, 15, and 20%, respectively). The causes of the central emitting wavelength shift are the temperature dependent emission spectra of Yb:LuAG and the intracavity intensity. For 1030 nm oscillation, the thermal population distribution and temperature dependent emission spectra of Yb:LuAG crystal play important roles on the central wavelength shift. However, for 1047 nm oscillation, the thermal population distribution at laser wavelength is weak comparing that at 1030 nm, therefore, the central wavelength shift of 1047 nm is smaller than that 1030 nm oscillation even though the intracavity intensity is higher. The central emitting wavelength shift observed in Yb:LuAG microchip lasers are in good agreement with those observed in Yb:Y_2O_3 [50] and Yb:YAG [51] ceramic lasers.

5. Conclusions

In conclusions, the microchip laser performance have been investigated by adopting Yb:LuAG crystals with different thickness at ambient temperature without active cooling of the gain media. Efficient laser performance of at 1030 and 1047 nm was achieved by using 5 at.% Yb:LuAG crystal, the slope efficiency of 72 and 54% was achieved with respect to the absorbed pump power for 1030 and 1047 nm oscillations. The shift of the central wavelength of these lasers is attributed to the intracavity intensity and temperature dependent emission spectra of Yb:LuAG, the higher the transmission of the output coupling, the shift of the central wavelength is less. The laser performance becomes worse with increase of the thickness of Yb:LuAG crystal at ambient temperature because the thermal properties of thick Yb:LuAG crystal are getting worse and reabsorption loss is large. Optimization of Yb:LuAG microchip lasers can be realized by adjusting the thickness of gain medium at ambient temperature without active cooling of the gain medium.

Acknowledgements This work was supported by the Program for New Century Excellent Talents in University (NCET) under Grant No. NCET-09-0669 and partially supported by the 21st Century Center of Excellence (COE) program of Ministry of Education, Science, Sports, and Culture of Japan. One of the authors (A.A.K.) wishes to acknowledge the Russian Foundation for Basic Research and the Russian Academy of Sciences.

References

[1] W.F. Krupke, IEEE J. Sel. Top. Quantum Electron. **6**, 1287 (2000).
[2] J. Dong, A. Shirakawa, K. Ueda, H. Yagi, T. Yanagitani, and A.A. Kaminskii, Appl. Phys. Lett. **89**, 091114 (2006).
[3] C. Hönninger, R. Paschotta, M. Graf, F. Morier-Genoud, G. Zhang, M. Moser, S. Biswal, J. Nees, A. Braun, G.A. Mourou, I. Johannsen, A. Giesen, W. Seeber, and U. Keller, Appl. Phys. B **69**, 3 (1999).
[4] P. Lacovara, H.K. Choi, C.A. Wang, R.L. Aggarwal, and T.Y. Fan, Opt. Lett. **16**, 1089 (1991).
[5] U. Brauch, A. Giesen, M. Karszewski, Chr. Stewen, and A. Voss, Opt. Lett. **20**, 713 (1995).
[6] T. Taira, J. Saikawa, T. Kobayashi, and R.L. Byer, IEEE J. Sel. Top. Quantum Electron. **3**, 100 (1997).
[7] H.W. Bruesselbach, D.S. Sumida, R.A. Reeder, and R.W. Byren, IEEE J. Sel. Top. Quantum Electron. **3**, 105 (1997).
[8] G.A. Bogomolova, D.N. Vylegzhanin, and A.A. Kaminskii, Sov. Phys. JETP **42**, 440 (1976).
[9] K. Sueda, S. Kawato, and T. Kobayashi, Laser Phys. Lett. **5**, 271 (2008).
[10] Yu. Senatsky, J.-F. Bisson, A. Shelobolin, A. Shirakawa, and K. Ueda, Laser Phys. **19**, 911 (2009).
[11] J. Dong, K. Ueda, A. Shirakawa, H. Yagi, T. Yanagitani, and A.A. Kaminskii, Opt. Express **15**, 14516 (2007).
[12] J. Dong, A. Shirakawa, S. Huang, Y. Feng, K. Takaichi, M. Musha, K. Ueda, and A.A. Kaminskii, Laser Phys. Lett. **2**, 387 (2005).
[13] G.J. Spühler, R. Paschotta, M.P. Kullberg, M. Graf, M. Moser, E. Mix, G. Huber, C. Harder, and U. Keller, Appl. Phys. B **72**, 285 (2001).

[14] T. Yubing, T. Huiming, P. Jiying, and L. HongYi, Laser Phys. **18**, 12 (2008).
[15] T.Y. Fan and J. Ochoa, IEEE Photon. Technol. Lett. **7**, 1137 (1995).
[16] T. Yubing, T. Huiming, C. Hongzhong, and M. Jieguang, Laser Phys. **18**, 15 (2008).
[17] Y.B. Tian, Z.H. Tian, H.M. Tan, and X.Y. Liu, Laser Phys. **20**, 793 (2010).
[18] H.Z. Cao, F.J. Liu, H.M. Tan, H.Y. Peng, M.H. Zhang, Y.Q. Chen, B. Zhang, B.L. Chen, and C.J. Wang, Laser Phys. **19**, 919 (2009).
[19] J. Dong, A. Shirakawa, and K.-I. Ueda, Appl. Phys. B **85**, 513 (2006).
[20] J. Dong, K. Ueda, H. Yagi, A.A. Kaminskii, and Z. Cai, Laser Phys. Lett. **6**, 282 (2009).
[21] D.C. Brown, IEEE J. Sel. Top. Quantum Electron. **11**, 587 (2005).
[22] J. Dong, M. Bass, Y.L. Mao, P.Z. Deng, and F.X. Gan, J. Opt. Soc. Am. B **20**, 1975 (2003).
[23] T.Y. Fan, D.J. Ripin, R.L. Aggarwal, J.R. Ochoa, B. Chann, M. Tilleman, and J. Spitzberg, IEEE J. Sel. Top. Quantum Electron. **13**, 448 (2007).
[24] J. Kawanaka, Y. Takeuchi, A. Yoshida, S.J. Pearce, R. Yasuhara, T. Kawashima, and H. Kan, Laser Phys. **20**, 1079 (2010).
[25] J. Dong and K. Ueda, Laser Phys. Lett. **2**, 429 (2005).
[26] A. Brenier and G. Boulon, Europhys. Lett. **55**, 647 (2001).
[27] L.D. DeLoach, S.A. Payne, L.L. Chase, L.K. Smith, W.L. Kway, and W.F. Krupke, IEEE J. Quantum Electron. **29**, 1179 (1993).
[28] A.A. Kaminskii, Laser Photon. Rev. **1**, 93 (2007).
[29] A.A. Kaminskii, Phys. Status Solidi (a) **97**, K53 (1986).
[30] A.A. Kaminskii, A.A. Markosyan, A.V. Pelevin, Y.A. Polaykova, S.E. Sarkisov, and T.V. Uvarova, Inorg. Mater. **22**, 773 (1986).
[31] K.S. Bagdasorov and A.A. Kaminskii, JETP Lett. **9**, 501 (1969).
[32] A.A. Kaminskii, A.O. Ivanov, S.E. Sarkisov, I.V. Mochalov, V.A. Fedorov, and L. Li, Sov. Phys. JETP **44**, 516 (1976).
[33] A.A. Kaminskii, Laser Crystals (Springer-Verlag, Berlin – Heidelberg – New York, 1981).
[34] R. Peters, C. Kränkel, K. Petermann, and G. Huber, Opt. Express **15**, 7075 (2007).
[35] A.A. Kaminskii, G.A. Bogomolova, K.S. Bagdasarov, and A.G. Petrosyan, Opt. Spectrosc. **39**, 1975 (1975).
[36] A.A. Kaminskii, K.S. Bagdasarov, A.G. Petrosyan, and S.E. Sarkisov, Phys. Status Solidi (a) **18**, K31 (1973).
[37] A.A. Kaminskii, P.V. Klevtsov, Kh.S. Bagdasarov, A.A. Maier, A.A. Pavlyuk, A.G. Petrosyan, and M.V. Provotorv, JETP Lett. **16**, 387 (1972).
[38] K.S. Bagdasarov, A.A. Kaminskii, A.M. Kevorkov, and A.M. Prokhorov, Sov. Phys. Dokl. **19**, 671 (1974).
[39] D.S. Sumida, T.Y. Fan, and R. Hutcheson, in: B.H.T. Chai and S.A. Payne (eds.), OSA Processings on Advanced Solid-State Lasers, Vol. 24 (Optical Society of America, 1995), p. 348.
[40] A. Brenier, Y. Guyot, H. Canibano, G. Boulon, A. Ródenas, D. Jaque, A. Eganyan, and A.G. Petrosyan, J. Opt. Soc. Am. B **23**, 676 (2006).
[41] T. Kasamatsu, H. Sekita, and Y. Kuwano, Appl. Opt. **38**, 5149 (1999).
[42] J. Dong, K. Ueda, and A.A. Kaminskii, Opt. Lett. **32**, 3266 (2007).
[43] J.P. He, X.Y. Liang, J.F. Li, H.B. Yu, X.D. Xu, Z.W. Zhao, J. Xu, and Z.Z. Xu, Opt. Express **17**, 11537 (2009).
[44] J. Saikawa, Y. Sato, T. Taira, and A. Ikesue, Appl. Phys. Lett. **85**, 1898 (2004).
[45] S. Kück, K. Petermann, U. Pohlmann, U. Schönhoff, and G. Huber, Appl. Phys. B **58**, 153 (1994).
[46] D.S. Sumida and T.Y. Fan, Opt. Lett. **19**, 1343 (1994).
[47] W.P. Risk, J. Opt. Soc. Am. B **5**, 1412 (1988).
[48] T. Fan and R. Byer, IEEE J. Quantum Electron. **23**, 605 (1987).
[49] W. Koechner, Solid State Laser Engineering (Springer-Verlag, Berlin, 1999).
[50] J. Kong, D.Y. Tang, J. Lu, and K. Ueda, Opt. Lett. **29**, 65 (2004).
[51] J. Dong, A. Shirakawa, K. Ueda, H. Yagi, T. Yanagitani, and A.A. Kaminskii, Opt. Lett. **32**, 1890 (2007).